

双包层椭圆光波导解析解*

董建峰 聂秋华

(宁波大学物理系, 宁波 315211)

摘 要 解析求解了双包层椭圆光纤中的波动方程, 得到了模式场精确解及模式特征方程。对基模的特征方程进行了数值计算, 给出了不同椭圆比下的归一化双折射和模间色散随归一化频率的变化关系曲线, 并与高斯近似解的结果进行了比较。

关键词 双包层椭圆光波导, 模式特征方程, 双折射, 模间色散。

1 引 言

保偏光纤有几何型^[1~4]和应力型^[5~7]两大类。有关研究表明, 由光纤几何不对称性制成的保偏光纤的温度稳定性比应力型保偏光纤好^[5~7]。几何型保偏光纤中最重要的一类是椭圆芯光纤。目前, 对单包层椭圆光纤, 理论和实验研究都已比较成熟^[1~4, 8~11], 而对双包层椭圆光纤, 虽然也有一些实验^[12]和理论研究^[13~14], 但理论研究只限于近似解法。对单包层椭圆光纤中的双折射的计算表明, 高斯近似解的结果与解析解的结果差一个约为 5/4 的因子。因此, 对双包层椭圆光纤进行解析解研究, 既有理论意义, 也有实际意义。本文在单包层椭圆光波导解析解研究^[10, 11]的基础上, 对双包层椭圆光纤中的波动方程进行了解析求解, 得到了模式场精确解及模式特征方程。对基模的特征方程进行了数值计算, 给出了不同椭圆比下的归一化双折射和模间色散随归一化频率的变化关系曲线, 并与高斯近似解法得出的结果进行了比较。

2 精确解和模式特征方程

对于由各向同性介质构成的双包层阶跃型椭圆光纤, 设纤芯、内包层、外包层折射率均匀分布, 分别为 n_0 、 n_1 、 n_2 , a_1 、 a_2 和 b_1 、 b_2 分别为纤芯、内包层截面椭圆的半长轴和半短轴, 双包层光纤截面椭圆边界由椭圆柱坐标中的 $\xi = \xi_1$ 、 $\xi = \xi_2$ 表示, 如图 1 所示。外包层可视为延伸到无穷远处。从麦克斯韦(Maxwell)方程出发, 可以得到光纤中的波动方程为

$$\nabla^2 V + k^2 V = 0 \quad (1)$$

式中, $k = nk_0$, 在纤芯中, $k = n_0 k_0$, 在内包层, $k = n_1 k_0$, 在外包层, $k = n_2 k_0$, k_0 是真空中波数, V 表示光纤中电磁场纵向分量 H_z 或 E_z 。

* 浙江省教委科研基金资助项目。

收稿日期: 1996 年 3 月 30 日; 收到修改稿日期: 1996 年 5 月 26 日

为求解椭圆光纤中波动方程的解, 采用椭圆柱坐标 (ξ, η, z) , (ξ, η, z) 与直角坐标的关系为:

$$\begin{cases} x = q \cosh \zeta \cos \eta \\ y = q \sinh \zeta \sin \eta \\ z = z \end{cases} \quad (\xi \geq 0, -\pi \leq \eta \leq \pi) \quad (2)$$

其中 $q = \sqrt{a_1^2 - b_1^2}$ 。假定 z 轴无限长, 则可以设波动方程的解为 $V(\zeta, \eta, z) = f(\zeta)g(\eta) \exp(i\beta z)$, 其中 β 为传播常数, 可以从边界条件导出。把此解代入波动方程, 分离变量后得到马修(Mathieu)方程和变型马修方程^[15]:

$$g''(\eta) + (\lambda - 2\gamma^2 \cos 2\eta)g(\eta) = 0 \quad (3)$$

$$f''(\zeta) - (\lambda - 2\gamma^2 \cosh 2\zeta)f(\zeta) = 0 \quad (4)$$

式中 λ 为分离变量常数, $\gamma^2 = q^2(k_0^2 n^2 - \beta^2)/4$, 在纤芯内 $(0 \leq \xi \leq \xi_1)$, $\gamma^2 = \gamma_0^2 = q^2(k_0^2 n_0^2 - \beta^2)/4$, 在内包层 $(\xi_1 \leq \xi \leq \xi_2)$, $-\gamma^2 = \gamma_1^2 = q^2(\beta^2 - k_0^2 n_1^2)/4$, 在外包层 $(\xi_2 \leq \xi < \infty)$, $-\gamma^2 = \gamma_2^2 = q^2(\beta^2 - k_0^2 n_2^2)/4$ 。

与单包层椭圆光波导^[10, 11]类似, 根据对马修方程和变型马修方程的解^[15]的分析, 可把双包层椭圆光纤中电磁场的纵向分量 H_z 和 E_z 写成马修函数和变型马修函数的形式。

奇模: (偶模的解只需 H_z 和 E_z 互换即可, 这里不再写出。)

$$\begin{cases} E_{z_0} = A_m C e_m(\zeta, \gamma_0^2) c e_m(\eta, \gamma_0^2) \exp(i\beta z) \\ H_{z_0} = B_m S e_m(\zeta, \gamma_0^2) s e_m(\eta, \gamma_0^2) \exp(i\beta z) \end{cases} \quad (0 \leq \zeta \leq \zeta_1) \quad (5)$$

$$\begin{cases} E_{z_1} = L_m K e_m(\zeta, \gamma_1^2) c e_m(\eta, -\gamma_1^2) \exp(i\beta z) \\ \quad + C_m I e_m(\zeta, \gamma_1^2) c e_m(\eta, -\gamma_1^2) \exp(i\beta z) \\ H_{z_1} = P_m K o_m(\zeta, \gamma_1^2) s e_m(\eta, -\gamma_1^2) \exp(i\beta z) \\ \quad + D_m I o_m(\zeta, \gamma_1^2) s e_m(\eta, -\gamma_1^2) \exp(i\beta z) \end{cases} \quad (\zeta_1 \leq \zeta \leq \zeta_2) \quad (6)$$

$$\begin{cases} E_{z_2} = F_m K e_m(\zeta, \gamma_2^2) c e_m(\eta, -\gamma_2^2) \exp(i\beta z) \\ H_{z_2} = G_m K o_m(\zeta, \gamma_2^2) s e_m(\eta, -\gamma_2^2) \exp(i\beta z) \end{cases} \quad (\zeta_2 \leq \zeta < \infty) \quad (7)$$

式中 $A_m, B_m, C_m, D_m, L_m, P_m, F_m, G_m$ 为待定常数, 它们之间的关系由边界条件决定。

可以证明, 当椭圆趋于圆时, 这些解与双包层圆光纤中的模式场解是一致的(文献[16]中的(7)(8)(9)式)。

根据电磁场横向分量与纵向分量之间的关系和切向分量连续的边界条件^[10, 11], 可以推出奇模的特征方程为:

$$\begin{vmatrix} g_{11} & g_{12} & g_{13} & g_{14} \\ g_{21} & g_{22} & g_{23} & g_{24} \\ g_{31} & g_{32} & g_{33} & g_{34} \\ g_{41} & g_{42} & g_{43} & g_{44} \end{vmatrix} = 0 \quad (8)$$

$$\begin{aligned} \text{其中} \quad g_{11} &= \frac{n_0 k_0}{\beta} \left(\frac{b_{10}}{b_{10}'} p_{11} + \frac{\gamma_0^2}{\gamma_1^2} p_{11}' \right) \frac{\beta_{10}}{\alpha_{10}}, & g_{12} &= \frac{\eta_0 k_0}{\beta} \left(\frac{b_{10}}{b_{10}'} d_{11} + \frac{\gamma_0^2}{\gamma_1^2} d_{11}' \right) \frac{\beta_{10}}{\alpha_{10}}, \\ g_{13} &= l_{11}(X_{00} + \gamma_0^2 W_{10}/\gamma_1^2 \alpha_{10}), & g_{14} &= c_{11} g_{13}/l_{11}, \end{aligned}$$

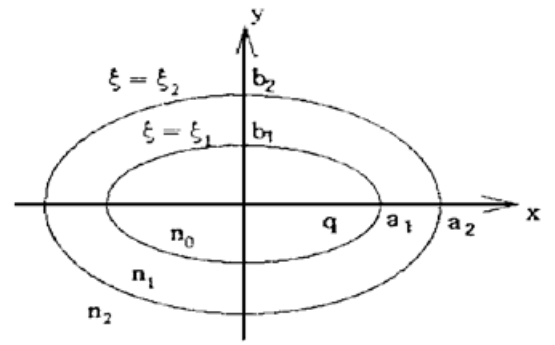


Fig. 1 The cross section of double-clad elliptical fibers

$$\begin{aligned}
g_{21} &= p_{11}(V_{00} + \gamma_0^2 \theta_{10} / \gamma_1^2 \beta_{10}), & g_{22} &= d_{11} g_{21} / p_{11}, \\
g_{23} &= -\frac{k_0}{\eta_0 \beta} (n_0^2 \frac{a'_{10}}{a_{10}} l_{11} + \frac{\gamma_0^2}{\gamma_1^2} n_1^2 l'_{11}) \frac{\alpha_{10}}{\beta_{10}}, & g_{24} &= -\frac{k_0}{\eta_0 \beta} (n_0^2 \frac{a'_{10}}{a_{10}} c_{11} + \frac{\gamma_0^2}{\gamma_1^2} n_1^2 c'_{11}) \frac{\alpha_{10}}{\beta_{10}}, \\
g_{31} &= \frac{\eta_0 k_0}{\beta} (p'_{21} - \frac{\gamma_1^2}{\gamma_2^2} p_{21} \frac{p'_{22}}{p_{22}}), & g_{32} &= \frac{\eta_0 k_0}{\beta} (d'_{21} - \frac{\gamma_1^2}{\gamma_2^2} d_{21} \frac{p'_{22}}{p_{22}}), \\
g_{33} &= l_{21}(X_{11} - \gamma_1^2 W_{21} / \gamma_2^2 \alpha_{21}), & g_{34} &= c_{21} g_{33} / l_{21}, \\
g_{41} &= p_{21}(V_{11} - \gamma_1^2 \theta_{21} / \gamma_2^2 \beta_{21}), & g_{42} &= d_{21} g_{41} / p_{21}, \\
g_{43} &= -\frac{k_0}{\eta_0 \beta} (n_1^2 l'_{21} - \frac{\gamma_1^2}{\gamma_2^2} n_2^2 l_{21} \frac{l'_{22}}{l_{22}}), & g_{44} &= -\frac{k_0}{\eta_0 \beta} (n_1^2 c'_{21} - \frac{\gamma_1^2}{\gamma_2^2} n_2^2 c_{21} \frac{l'_{22}}{l_{22}}).
\end{aligned}$$

偶模的特征方程为:

$$\begin{vmatrix} h_{11} & h_{12} & g_{13} & g_{14} \\ g_{21} & g_{22} & h_{23} & h_{24} \\ h_{31} & h_{32} & g_{33} & g_{34} \\ g_{41} & g_{42} & h_{43} & h_{44} \end{vmatrix} = 0 \quad (9)$$

其中

$$\begin{aligned}
h_{11} &= -\frac{k_0}{\eta_0 \beta} (n_0^2 \frac{b'_{10}}{b_{10}} p_{11} + \frac{\gamma_0^2}{\gamma_1^2} n_1^2 p'_{11}) \frac{\beta_{10}}{\alpha_{10}}, & h_{12} &= -\frac{k_0}{\eta_0 \beta} (n_0^2 \frac{b'_{10}}{b_{10}} d_{11} + \frac{\gamma_0^2}{\gamma_1^2} n_1^2 d'_{11}) \frac{\beta_{10}}{\alpha_{10}}, \\
h_{23} &= \frac{\eta_0 k_0}{\beta} (\frac{a'_{10}}{a_{10}} l_{11} + \frac{\gamma_0^2}{\gamma_1^2} l'_{11}) \frac{\alpha_{10}}{\beta_{10}}, & h_{24} &= \frac{\eta_0 k_0}{\beta} (\frac{a'_{10}}{a_{10}} c_{11} + \frac{\gamma_0^2}{\gamma_1^2} c'_{11}) \frac{\alpha_{10}}{\beta_{10}}, \\
h_{31} &= -\frac{k_0}{\eta_0 \beta} (n_1^2 p'_{21} - \frac{\gamma_1^2}{\gamma_2^2} n_2^2 p_{21} \frac{p'_{22}}{p_{22}}), & h_{32} &= -\frac{k_0}{\eta_0 \beta} (n_1^2 d'_{21} - \frac{\gamma_1^2}{\gamma_2^2} n_2^2 d_{21} \frac{p'_{22}}{p_{22}}), \\
h_{43} &= \frac{\eta_0 k_0}{\beta} (l'_{21} - \frac{\gamma_1^2}{\gamma_2^2} l_{21} \frac{l'_{22}}{l_{22}}), & h_{44} &= \frac{\eta_0 k_0}{\beta} (c'_{21} - \frac{\gamma_1^2}{\gamma_2^2} c_{21} \frac{l'_{22}}{l_{22}}).
\end{aligned}$$

式中 $\eta_0 = \sqrt{\mu_0 / \epsilon_0}$ 为真空中的波阻抗, 其它参数定义见附录, 带撇的为相应的导数值。

可以证明, 当 $\zeta = \zeta_c$ 或 $n_0 = n_1$ 或 $n_1 = n_2$ 时, 方程变成单包层的特征方程。当 $a_1 = b_1$, $a_2 = b_2$ 时, 方程变成圆的双包层的特征方程(文献[16]中的(17)式)。

3 数值计算结果和讨论

在(5)~(9)式中, 令 $m = 1$, 即得基模的模式场解和特征方程。基模的奇模和偶模特征方程, 是包含马修函数的超越方程, 只能利用计算机进行数值求解。模式特征方程中只包含一个未知量 β , 可用弦截法求解, 包含角向马修函数的参数利用辛普生数值积分方法计算, 在计算过程中, 必须调用马修函数组成的函数库^[10, 11]。

作为例子, 本文对基模的奇模和偶模特征方程进行了数值求解, 得到了精确的传播常数 β_o 、 β_e , 进而求出了归一化双折射 $B = (\beta_o - \beta_e) / k_0$, 模间色散 $\Delta\tau = (1/c) \partial(\beta_o - \beta_e) / \partial k$ 随归一化频率 $V_y = k_0 b_1 \sqrt{n_0^2 - n_2^2}$ 的变化关系。

首先比较了利用本文得到的精确解和用高斯近似解对单包层椭圆光纤($n_1 = n_2$) 的双折射的计算结果, 如图2所示。从图中可以看出, 随着椭圆比的增大, B / Δ^2 [$\Delta = (n_0^2 - n_2^2) / 2n_0^2$] 增大, 而且最大值位置移向低频端。对于一定的 V_y 值, 当 Δ 从 0.001 变化到 0.07 时, B / Δ^2 基本不变。图2虚线是用高斯近似解得出的结果, 对于相同的椭圆比, 双折射的最大值只有精确解的 80% 左右, 这一点与文献[14]的结果不同, 最大值位置也有所不同。(顺便指出, 文献

[14] 中的图 4 是错误的, 并且和图 5 是相互矛盾的。)

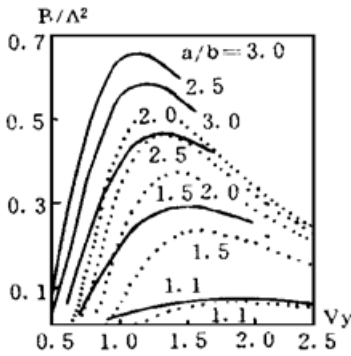


Fig. 2 Normalized birefringence B/Δ^2 of single-clad elliptical fibers as a function of normalized frequency V_y for different aspect ratios a/b . (Solid and dashed lines correspond to exact solution and Gaussian approximation.)

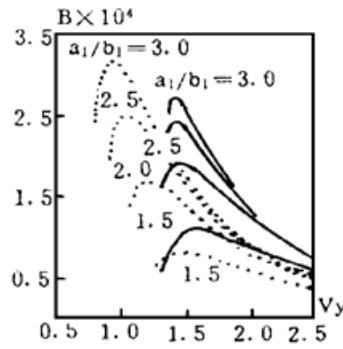


Fig. 3 Normalized birefringence B of double-clad elliptical fibers as a function of normalized frequency V_y for different aspect ratios a/b . (Solid and dashed lines correspond to exact solution and Gaussian approximation.)

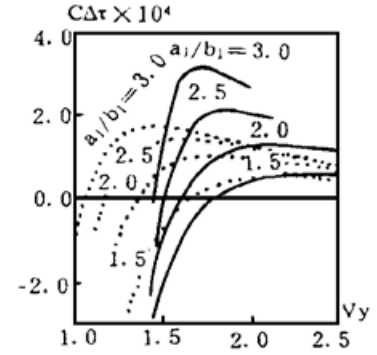


Fig. 4 Modal dispersion $c\Delta\tau$ of double-clad elliptical fibers as a function of normalized frequency V_y for different aspect ratios a/b . (Solid and dashed lines correspond to exact solution and Gaussian approximation.)

图 3 表示双包层椭圆光纤的归一化双折射 B 随归一化频率 V_y 的变化关系曲线, 图中设 $\Delta_1 = (n_0^2 - n_1^2)/2n_0^2 = 0.027$, $\Delta_2 = (n_0^2 - n_2^2)/2n_0^2 = 0.01$, $R_x = a_1/b_1 = 1.2$ 。由图可知, 双折射的最大值位置与单包层的相比, 移向高频端。计算发现, 双折射的大小随 Δ_1 的增大而增大, 对于以上所设, 双折射的最大值约为单包层的 5 倍左右。高斯近似解与精确解相比较, 双折射的最大值位置和大小都有比较大的差别, 最大值位置的 V_y 值偏小, 对于较小的椭圆比, 大小也只有精确解的 80% 左右。而对较大的椭圆比, 其值反而偏大。

图 4 表示双包层椭圆光纤的模间色散 $c\Delta\tau$ 随归一化频率 V_y 的变化关系曲线。图中也设 $\Delta_1 = 0.027$, $\Delta_2 = 0.01$, $R_x = 1.2$ 。从图可以看出, 在不同椭圆比下达到零色散是可能的, 但零色散的 V_y 值位置比高斯近似解的大, 对于大的椭圆比, 并不在单模区。这一点与高斯近似解法得到的结论也不同^[14]。

结 论 本文在单包层椭圆光波导解析解研究的基础上, 对双包层椭圆光纤中的波动方程进行了解析求解, 得到了模式场精确解及模式特征方程。对基模的特征方程进行了数值计算, 给出了不同椭圆比下的归一化双折射和模间色散随归一化频率的变化关系曲线, 并与高斯近似解法得出的结果进行了比较。

参 考 文 献

- [1] C. Yeh, Elliptical dielectric waveguides. *J. Appl. Phys.*, 1962, **33**(11): 3235~ 3243
- [2] R. E. Dyott, J. R. Cozens, D. G. Morris, Preservation of polarization in optical-fiber waveguides with elliptical cores. *Electron. Lett.*, 1979, **15**(13): 380~ 382
- [3] S. C. Rashleigh, M. J. Marrone, Polarization holding in elliptical-core birefringence fibers. *IEEE J. Quant. Electron.*, 1982, **QE-18**(12): 1515~ 1523
- [4] V. Ramaswamy, W. G. French, R. D. Standley, Polarization characteristics of noncircular core single-mode fibers. *Appl. Opt.*, 1978, **17**(18): 3014~ 3017
- [5] V. Ramaswamy, R. H. Stolen, M. D. Divine et al., Birefringence in elliptically clad borosilicate single-mode fibers. *Appl. Opt.*, 1979, **18**(24): 4080~ 4084

- [6] S. C. Rashleigh, M. J. Marrone, Polarization-holding in a high-birefringence fiber. *Electron. Lett.*, 1982, **18**(8) : 326~ 327
- [7] T. Hosaka, Y. Sasaki, J. Noda *et al.*, Low-loss and low-crosstalk polarization-maintaining optical fibers. *Electron. Lett.*, 1985, **21**(19) : 920~ 921
- [8] A. Kumar, R. K. Varshney, K. Thyagarajan, Birefringence calculations in elliptical-core optical fibers. *Electron. Lett.*, 1984, **20**(3) : 112~ 113
- [9] S. N. Sarkar, K. Thyagarajan, A. Kumar, Gaussian approximation of the fundamental mode in single clad elliptical core fibers. *Opt. Commun.*, 1984, **49**(3) : 178~ 183
- [10] 聂秋华, 董建峰, 叶庆卫, 椭圆光波导基模解析解研究. 宁波大学学报, 1995, **8**(1) : 38~ 43
- [11] 董建峰, 聂秋华, 椭圆光波导解析解及第一个高阶模的截止频率研究. 光通信研究, 1995, **21**(3) : 35~ 39
- [12] R. K. Varshney, R. Srivastava, R. V. Ramaswamy, Characterization of highly elliptical submicron core polarization preserving fibers: theory and experiment. *Appl. Phys.*, 1988, **27**(15) : 3114~ 3120
- [13] R. K. Varshney, A. Kumar, Effect of depressed inner cladding on the polarization characteristics of elliptical core fibers. *Opt. Lett.*, 1984, **9**(11) : 522~ 525
- [14] F. Zhang, J. W. Y. Lit, Polarization characteristics of double-clad elliptical fibers. *Appl. Opt.*, 1990, **29**(36) : 5336~ 5342
- [15] Edited by Milton Abramowitz, Irene A. Stegun, *Handbook of Mathematical Functions*. New York, Dover Publications, Inc., 1965, 721~ 750
- [16] S. Kawakami, S. Nishida, Characteristics of a doubly clad optical fiber with a low-index inner cladding. *IEEE J. Quant. Electron.*, 1974, **QE-10**(12) : 879~ 887

附录:

正文中所用的参数定义如下:

$$\begin{aligned}
 a_{10} &= C e_m(\zeta, \gamma_0^2), & b_{10} &= S e_m(\zeta, \gamma_0^2), & l_{11} &= K e_m(\zeta, \gamma_1^2), & p_{11} &= K o_m(\zeta, \gamma_1^2), \\
 c_{11} &= I e_m(\zeta, \gamma_1^2), & d_{11} &= I o_m(\zeta, \gamma_1^2), & l_{21} &= K e_m(\zeta, \gamma_1^2), & p_{21} &= K o_m(\zeta, \gamma_1^2), \\
 c_{21} &= I e_m(\zeta, \gamma_1^2), & d_{21} &= I o_m(\zeta, \gamma_1^2), & l_{22} &= K e_m(\zeta, \gamma_2^2), & p_{22} &= K o_m(\zeta, \gamma_2^2),
 \end{aligned}$$

$$\alpha_{10} = \frac{\int_0^{2\pi} c e_m(\eta, -\gamma_1^2) c e_m(\eta, \gamma_0^2) d\eta}{\int_0^{2\pi} c e_m^2(\eta, \gamma_0^2) d\eta}, \quad \beta_{10} = \frac{\int_0^{2\pi} s e_m(\eta, -\gamma_1^2) s e_m(\eta, \gamma_0^2) d\eta}{\int_0^{2\pi} s e_m^2(\eta, \gamma_0^2) d\eta},$$

$$X_{00} = \frac{\int_0^{2\pi} c e_m'(\eta, \gamma_0^2) s e_m(\eta, \gamma_0^2) d\eta}{\int_0^{2\pi} s e_m^2(\eta, \gamma_0^2) d\eta}, \quad V_{00} = \frac{\int_0^{2\pi} s e_m'(\eta, \gamma_0^2) c e_m(\eta, \gamma_0^2) d\eta}{\int_0^{2\pi} c e_m^2(\eta, \gamma_0^2) d\eta},$$

$$W_{10} = \frac{\int_0^{2\pi} c e_m'(\eta, -\gamma_1^2) s e_m(\eta, \gamma_0^2) d\eta}{\int_0^{2\pi} s e_m^2(\eta, \gamma_0^2) d\eta}, \quad \theta_{10} = \frac{\int_0^{2\pi} s e_m'(\eta, -\gamma_1^2) c e_m(\eta, \gamma_0^2) d\eta}{\int_0^{2\pi} c e_m^2(\eta, \gamma_0^2) d\eta},$$

$$\alpha_{21} = \frac{\int_0^{2\pi} c e_m(\eta, -\gamma_2^2) c e_m(\eta, \gamma_1^2) d\eta}{\int_0^{2\pi} c e_m^2(\eta, -\gamma_1^2) d\eta}, \quad \beta_{21} = \frac{\int_0^{2\pi} s e_m(\eta, -\gamma_2^2) s e_m(\eta, -\gamma_1^2) d\eta}{\int_0^{2\pi} s e_m^2(\eta, \gamma_1^2) d\eta},$$

$$\begin{aligned}
 X_{11} &= \frac{\int_0^{2\pi} ce'_m(\eta, -\gamma_1^2) se_m(\eta, -\gamma_1^2) d\eta}{2\pi \int_0^{2\pi} se_m^2(\eta, -\gamma_1^2) d\eta}, & V_{11} &= \frac{\int_0^{2\pi} se'_m(\eta, -\gamma_1^2) ce_m(\eta, -\gamma_1^2) d\eta}{2\pi \int_0^{2\pi} ce_m^2(\eta, -\gamma_1^2) d\eta}, \\
 W_{21} &= \frac{\int_0^{2\pi} ce'_m(\eta, -\gamma_2^2) se_m(\eta, -\gamma_1^2) d\eta}{2\pi \int_0^{2\pi} se_m^2(\eta, -\gamma_1^2) d\eta}, & \theta_{21} &= \frac{\int_0^{2\pi} se'_m(\eta, -\gamma_2^2) ce_m(\eta, -\gamma_1^2) d\eta}{2\pi \int_0^{2\pi} ce_m^2(\eta, -\gamma_1^2) d\eta}.
 \end{aligned}$$

Analytical Solutions of Double-Clad Elliptical Optical Waveguide

Dong Jianfeng Nie Qihua

(Department of Physics, Ningbo University, Ningbo, 315211)

(Received 30 March 1996; revised 26 May 1996)

Abstract The analytical solutions of electromagnetic wave equations for double-clad elliptical optical waveguide have been studied. The mode field distribution and the mode characteristic equations are obtained. The numerical solution for characteristic equations of fundamental modes are derived. The normalized birefringence and modal dispersion as functions of normalized frequency for different aspect ratios are presented and compared with Gaussian approximation.

Key words double-clad elliptical optical waveguide, mode characteristic equations, normalized birefringence, modal dispersion.